JOURNAL OF CATALYSIS 140, 136–149 (1993)

An Auger Electron Spectroscopy Study of the Activation of Iron Fischer–Tropsch Catalysts

II. Carbon Monoxide Activation[1]

ALLEN G. SAULT* AND ABHAYA K. DATYE†

*Fuel Science Department 6211, Sandia National Laboratories, Albuquerque, New Mexico 87185; and †Department of Chemical and Nuclear Engineering, University of New Mexico, Albuquerque, New Mexico 87131

Received June 23, 1992; revised October 29, 1992

Activation procedures can have a dramatic effect on the activity of iron-based catalysts for Fischer–Tropsch (F–T) synthesis. CO conversion over a 100 Fe/3 Cu/0.2 K catalyst (parts by weight) can vary by nearly a factor of 3, depending on activation treatment. In contrast, a 100 Fe/5 Cu/4.2 K/25 SiO_2 catalyst displays little dependence of F–T activity on activation treatment. An ultra-high vacuum surface analysis chamber coupled to an atmospheric reactor has been used to measure the surface composition of these catalysts following activation in carbon monoxide at 280°C, while transmission electron microscopy (TEM) and BET surface area measurements have been used to investigate catalyst morphology. CO activation of the 100 Fe/5 Cu/4.2 K/25 SiO_2 catalyst at 280°C results in partial reduction of iron to a mixture of Fe_xO and Fe_3O_4, and an overall surface composition very similar to that obtained following hydrogen activation at 220 or 280°C, consistent with the invariance of F–T activity with activation treatment for this catalyst. Activation of the 100 Fe/3 Cu/0.2 K catalyst in CO at 280°C results in the formation of iron carbide particles, growth of graphitic carbon (C_g) filaments, and formation of a thick, porous, C_g layer covering the carbide particles. Differences in F–T activity between the hydrogen- and CO-activated 100 Fe/3 Cu/0.2 K catalyst are discussed in terms of surface composition and catalyst morphology. The difference in sensitivity of the two catalysts to activation conditions is related to differences in the extent of reduction of the catalysts.

1. INTRODUCTION

In the previous paper (*1*), the effects of activation in hydrogen on the surface compositions of two iron Fischer–Tropsch (F–T) catalysts were examined. Although the two catalysts, with compositions of 100 Fe/3 Cu/0.2 K and 100 Fe/5 Cu/4.2 K/25 SiO_2 (parts by weight), display widely differing behavior with respect to hydrogen activation, good correlations were found between catalyst surface composition and F–T activity in both cases. In this paper, the study of the activation of these two catalysts is extended to include the effects of activation in CO.

Activation in CO is potentially more complicated than activation in hydrogen. While both CO and hydrogen activation can result in reduction of iron oxides, thermodynamic calculations show that reduction by CO is more favorable than reduction in hydrogen (*2*), a prediction supported by temperature-programmed reduction (TPR) studies (*3–5*). In addition to iron reduction, CO activation can lead to the deposition of carbon *via* the Boudouard reaction, in which CO disproportionates to form carbon and CO_2. The form in which carbon exists on the iron surface has important consequences for catalyst performance. Carbidic carbon deposition is considered advantageous, while graphitic carbon deposition is believed to poison catalyst activity (*6, 7*). Within the context of the competition model proposed by Niemantsverdriet *et al.* (*8, 9*), the purpose of CO activation is to

[1] This work was performed at Sandia National Laboratories for the U.S. Department of Energy under Contract DE-AC04-76DP000789.

0021-9517/93 $5.00

precarbide the iron catalyst and avoid the induction period often observed during the initial stages of iron F–T catalyst testing (*6, 9–12*). The competition model assumes that carbon atoms deposited on the surface of a reduced iron catalyst during F–T synthesis can follow three different reaction pathways: (i) reaction with metallic iron to form iron carbides, (ii) reaction with adsorbed hydrogen to form hydrocarbons, and (iii) conversion to inactive (graphitic) carbon. In the initial stages of F–T synthesis, reaction (i) is much faster than the other reactions, and most of the carbon is consumed in the formation of iron carbides. As a result, initial rates of F–T synthesis are very slow. As the reaction proceeds, the bulk of the iron becomes carbided, decreasing the rate of reaction (i) such that reactions (ii) and (iii) become competitive. The net result of these processes is a maximum in the rate of reaction (ii) with time. By activating catalysts in CO or H_2/CO mixtures, carbide formation can potentially be accomplished during the activation treatment, thereby avoiding the induction period during the initial stages of F–T synthesis.

The two catalysts used in this study display different sensitivities to activation procedures, as shown in Table 1. The F–T activity and selectivity of the 100 Fe/5 Cu/4.2 K/25 SiO_2 catalyst is fairly independent of activation procedure. Initial CO conversions of 55–65% are obtained following either CO or hydrogen activation when F–T activity is measured in a fixed bed reactor at 250°C, 1.48 MPa, H_2:CO = 2:3, and a space velocity of 2 Nl/g catalyst·h (*13*). The F–T activity and selectivity of the 100 Fe/3 Cu/0.2 K catalyst, however, is strongly dependent on activation procedure. Initial CO conversion, measured in a fixed bed reactor at 250°C, 1.48 MPa, H_2:CO = 1:1, and a space velocity of 2 Nl/g catalyst·h varies from 30 to 80% depending on activation procedure, with CO activation at 280°C and 0.1 MPa (1 atm) for 24 h resulting in the highest activity (*14*). Consequently, it is expected that CO activation of the 100 Fe/5 Cu/4.2 K/25 SiO_2 catalyst should result in a surface composition similar to that observed following hydrogen activation, while CO activation of the 100 Fe/3 Cu/0.2 K catalyst should result in a surface composition which is substantially different from that observed following hy-

TABLE 1

CO Conversion *vs* Activation for 100 Fe/3 Cu/0.2 K and 100 Fe/5 Cu/4.2 K/25 SiO_2 Catalysts

Activation treatment	Initial CO conversion (%)	Hydrocarbon selectivities (wt%)			
		CH_4	C_2–C_4	C_5–C_{11}	C_{12}^+
100 Fe/5 Cu/4.2 K/25 SiO_2[a]					
CO, 280°C, 12 h	55	5	22	19	54
H_2, 220°C, 1 h	59	6	21	29	44
H_2, 280°C, 1 h	64	9	24	47	20
100 Fe/3 Cu/0.2 K[b]					
CO, 280°C, 8 h	80	7	27	31	35
CO, 280°C, 24 h	80	7	26	23	44
H_2, 250°C, 8 h	66	14	40	39	7
H_2, 250°C, 24 h	60	12	39	42	7
H_2, 280°C, 8 h	44	14	45	37	4
H_2, 280°C, 24 h	30	11	39	40	10

[a] 250°C, 1.48 MPa, H_2:CO = 2:3, 2 Nl/g-catalyst·h, from Ref. (*13*).
[b] 250°C, 1.48 MPa, H_2:CO = 1:1, 2 Nl/g-catalyst·h, from Ref. (*14*).

drogen activation. The results presented in this paper confirm these expectations, and also aid in understanding the difference in sensitivity of the two catalysts to activation procedures and the reasons for the activity trends observed for the 100 Fe/3 Cu/0.2 K catalyst.

2. METHODS

Details of the experimental apparatus and procedures are given in the previous paper (*1*). Briefly, the system consists of an ultra-high vacuum (UHV) surface analysis chamber coupled to an atmospheric pressure reactor, which allows catalyst samples to be subjected to realistic activation or reaction conditions, and then transferred into UHV for surface analysis. Transfer is accomplished without exposure of the samples to air, thereby avoiding any possible alteration of catalyst surface composition by reaction with ambient oxygen. This capability is crucial to obtaining relevant information on the surface composition of working catalysts, as activated catalysts are often highly reactive toward oxygen. Auger electron spectroscopy (AES) is the primary surface analytical technique employed in this study, and details of the data acquisition and analysis procedures are given in the previous paper (*1*).

The two catalysts studied have compositions of 100 Fe/3 Cu/0.2 K and 100 Fe/5 Cu/4.2 K/25 SiO_2. The 100 Fe/5 Cu/4.2 K/25 SiO_2 catalyst is a commercial catalyst manufactured by Ruhrchemie. Details of catalyst preparation procedures can be found elsewhere (*3*, *14*), while sample mounting and outgassing procedures are described in the previous paper (*1*). The catalyst samples were heated to 300°C in 130 Torr O_2 for 3 h prior to activation in CO in order to simulate the calcining step employed by Bukur *et al.* (*14*) in their activity measurements. At least three different samples were studied for each catalyst to ensure that the results were representative, and not due to artifacts associated with a particular catalyst sample. Prior to introduction into the reactor, CO (Alphagaz, Research Grade) was passed through a liquid-nitrogen-cooled U-tube packed with glass wool in order to remove metal carbonyls. The reactor was filled at a rate of <1 Torr/s, since it was found that higher fill rates resulted in inefficient removal of carbonyls by the liquid-nitrogen trap. The presence of carbonyls in the reactor was easily detected by deposition of nickel on the catalyst surface. Any data which showed Auger transitions characteristic of nickel were therefore rejected as being compromised by the presence of nickel and iron carbonyls. The slow fill rates needed to avoid carbonyl contamination meant that >10 min were required to fill the reactor to atmospheric pressure (630 Torr in Albuquerque). Since CO activation generally lasted for many hours, the time required to fill the reactor is not significant. After the reactor was evacuated and the gate valve was opened to the UHV chamber following activation, the analysis chamber pressure typically rose to $>1 \times 10^{-7}$ Torr, consisting mainly of water, but with substantial amounts of CO and CO_2. Water arises from outgassing of the sample during activation, while CO_2 arises from reduction of iron oxides, and from the Boudouard reaction in which CO disproportionates to form CO_2 and surface carbon. As was the case for hydrogen activation, the catalyst samples, which were smooth red-brown pellets initially, shrank and cracked during CO activation and changed to a deep black color.

A flow reactor consisting of a glass U-tube with a sintered glass frit enclosed by an oven was used to prepare samples of the 100 Fe/3 Cu/0.2 K catalyst for transmission electron microscopy (TEM) and BET surface area analysis. One gram of the catalyst was first heated in air (calcined) at 300°C for 5 h in a muffle furnace, and then heated to 280°C in CO flowing at 150 sccm for 24 h in the U-tube reactor. Metal carbonyls were removed prior to contact with the sample by passing the CO over a high-surface-area silica heated to 300°C. During the first 30

min of activation, the sample temperature rose to ~335°C indicating the occurrence of an exothermic reaction. Following activation, the sample was cooled to room temperature in CO, and then passivated in 2.0 Torr of air overnight. The 100 Fe/3 Cu/0.2 K sample changed from reddish-brown to deep black during activation in CO, and exhibited a 91% weight gain. BET analysis was performed using a Quantachrome Autosorb-6. TEM pictures were obtained on a JEM 2000 FX microscope operated at 200 kV. Samples were supported on holey carbon films mounted on 3-mm Cu grids.

3. RESULTS AND DISCUSSION

3.1. 100 Fe/5 Cu/4.2 K/25 SiO_2 Catalyst

Figure 1 shows the Auger spectrum of the 100 Fe/5 Cu/4.2 K/25 SiO_2 catalyst following activation in CO at 280°C for 12 h. Also shown in Fig. 1 for comparison is the spectrum of the same catalyst activated in hydrogen for 1 h at 200°C (*1*). The two spectra are nearly identical, consistent with the fact that the two activation procedures result in catalysts with nearly identical F–T activities and selectivities (*13*). Both spectra display peaks due to iron, oxygen, potassium, silicon, and copper, although the Cu(920 eV) signal is difficult to discern with the signal-to-noise ratio in Fig. 1. The peak shapes and relative peak heights for the various elements are discussed in detail in the preceding paper (*1*), where it was noted that the presence of two peaks at 43 and 52 eV in the Fe(MVV) region of the spectra indicate that oxidized iron is present, most likely as a mixture of Fe_xO and Fe_3O_4. No evidence exists for the presence of metallic iron on the surface following either hydrogen or CO activation. It is important to note that no carbon deposition occurs during CO activation of this catalyst. As discussed in the Introduction, carbon deposition during CO activation can have an effect on initial F–T activity. The absence of carbon deposition is discussed in Section 3.3.

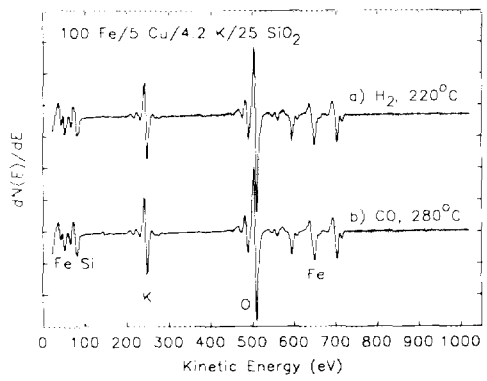

Fig. 1. Auger spectra of the 100 Fe/5 Cu/4.2 K/25 SiO_2 catalyst following (a) activation in 1 atm of hydrogen at 220°C for 1 h and (b) activation in one atmosphere of CO at 280°C for 12 h. Spectra are normalized to the Fe(703 eV) peak.

In contrast to the present work, Li (*3*) reports that approximately 30% of the iron in a 100 Fe/5 Cu/4.2 K/25 SiO_2 catalyst similar to the one used here is reduced to the metallic state following reduction in CO at 300°C for 12 h. Li also reports a large C(1*s*) peak at 284–285 eV; however, a large carbon peak was observed following hydrogen activation as well, indicating that the carbon is largely adventitious and not the result of CO activation. The slightly higher activation temperature used in the XPS studies could account for the increased extent of reduction observed by XPS compared to the present AES results. Also, differences in surface sensitivity between the XPS and AES must be considered when comparing results from the two techniques. With the Al $K\alpha$ X-ray source used by Li, the Fe $2p_{3/2}$ photoelectrons used to determine oxidation state would have kinetic energies of ~775 eV, giving them an inelastic mean free path (IMFP) in a mixture of Fe_xO and Fe_3O_4 of ~2 nm, *vs* only 0.7 nm for the 47 eV Fe(MVV) Auger electrons (*15*). As a result, XPS is less surface sensitive than AES for iron oxidation state measurements. Thus, metallic iron residing below a surface oxide phase would be more likely to be detected by Li using XPS, than by the AES technique employed here. The possibility of a metallic iron phase underlying a

surface oxide was raised by Lox *et al.* (*16*), for hydrogen activation at 220°C of the 100 Fe/5 Cu/4.2 K/25 SiO_2 catalyst. As a final comment on Li's work, it should be noted that no attempt appears to have been made to distinguish metallic iron from iron carbide. Iron carbide displays an Fe $2p_{3/2}$ peak shape nearly identical to that of iron metal, but the peak is shifted 0.2–0.3 eV to higher energy (*6, 17*). It is therefore entirely possible that Li actually detected an underlying carbide phase, rather than metallic iron following CO activation of the 100 Fe/5 Cu/4.2 K/25 SiO_2 catalysts. In support of this possibility are the results of Kuivila *et al.* (*12*), who found that F–T synthesis over an unreduced Fe_2O_3 catalyst results in greater carbide levels in the bulk than on the surface. If a similar situation exists for the CO activated 100 Fe/5 Cu/4.2 K/25 SiO_2 catalyst, then the XPS studies may have detected metallic or carbided iron residing below a surface oxide phase, while the greater surface sensitivity of AES prevented the detection of the bulk iron phase in the present work.

As was the case for hydrogen activation of the 100 Fe/5 Cu/4.2 K/25 SiO_2 catalyst (*1*), removal of potassium and silica by electron beam effects results in an increase in the ease of reduction of iron during CO activation. For activation in CO at 280°C for 6 h, Fig. 2 shows that decreased potassium and silica coverages result in a corresponding decrease in the O(511 eV)/Fe(703 eV) ratio, as well as changes in the Fe(MVV) peak shape which are consistent with increased reduction of iron (*18–21*). It has been shown previously that both potassium (*3, 22*) and silica (*3, 22–24*) can inhibit reduction of iron F–T catalysts. The effects of potassium and silica cannot be separated in the present work, since no method is available which would remove one of the components while leaving the coverage of the second component unchanged.

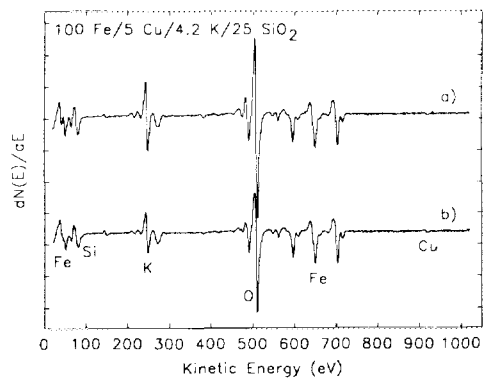

FIG. 2. Effect of lowering silica and potassium levels on the Auger spectrum of the 100 Fe/5 Cu/4.2 K/25 SiO_2 catalyst following activation in one atmosphere of CO for 6 h at 250°C. Spectra are normalized to the Fe(703 eV) peak.

3.2. *100 Fe/3 Cu/0.2 K Catalyst*

3.2.1. Auger electron spectroscopy and transmission electron microscopy. Figure 3 shows the effects of CO activation at 280°C on the surface composition of the 100 Fe/3 Cu/0.2 K catalyst. The largest peak in the spectra in Fig. 3 is due to carbon at 272 eV, and the C(272 eV)/Fe(703 eV) peak ratio grows with activation time. The featureless, assymetric shapes of these carbon peaks are in good agreement with the peak shapes reported by Wesner *et al.* (*25*) for mixed potassium/graphitic carbon overlayers on an iron foil. No fine structure is present on the low energy side of the C(272 eV) peaks to suggest the presence of carbidic carbon (*25, 26*). Although overlap with the potassium peak at 250 eV might prevent the detection of a small amount of carbidic carbon, it is nevertheless clear that the vast majority of the carbon on the surface is graphitic (C_g). In addition to the carbon peaks, peaks due to copper, potassium, iron and oxygen are also visible in the spectra of Fig. 3, as expected. These components will be discussed in more detail below. Note that the Fe(MVV) peak at 47 eV is completely attenuated by the C_g overlayer. The peaks which are visible below 100 eV varied in size, shape and position with carbon coverage, and are probably due to low energy carbon Auger transitions.

While Fig. 3 provides information on the

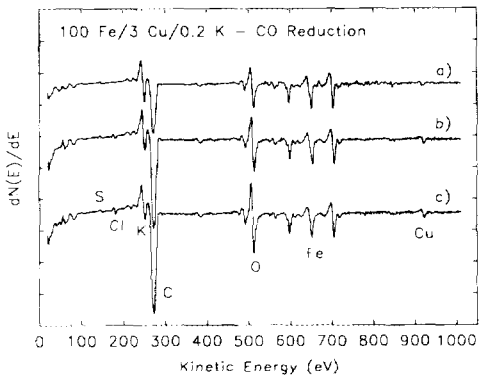

FIG. 3. Auger spectra of 100 Fe/3 Cu/0.2 K catalyst following activation in one atmosphere of CO at 280°C for (a) 4 h, (b) 10 h, and (c) 22 h. Spectra are normalized to the Fe(703 eV) peak.

surface composition of the CO activated 100 Fe/3 Cu/0.2 K catalyst, information regarding catalyst morphology is contained in the electron micrographs and diffraction patterns shown in Fig. 4. Prior to activation in CO, little structure is visible in the calcined catalyst (Fig. 4a). Those particles which can be discerned are on the order of 10 nm in size. Based on this particle size and a density of 5.24 g/cm^3 for Fe_2O_3, the surface area of the calcined 100 Fe/3 Cu/0.2 K catalyst is predicted to be approximately 115 m^2/g, in good agreement with the value of 139 m^2/g obtained from the BET measurement. The electron diffraction pattern prior to CO activation shows the presence of diffraction rings due to α-Fe_2O_3, as expected for a calcined iron catalyst.

After activation in CO and the subsequent passivation step, major changes can be observed in both the electron micrograph and the diffraction pattern (Fig. 4b). The electron micrograph shows the presence of 20–100 nm particles, with an average size of ~50 nm, indicating that some sintering occurs during CO activation. All of the particles are encapsulated by a second phase with a thickness varying from 2 to 15 nm. In addition, some of the smaller particles are located on the ends of long filaments. The diffraction pattern shows rings which can be ascribed either to graphitic carbon or iron carbide. No rings due to metallic iron or iron oxide are observed. Based on the electron diffraction results, as well as the AES results presented above, the encapsulating phase and filaments are identified as graphitic carbon, while the particles are an unidentified iron carbide. Overlap between the graphite and carbide rings, and the fact that all iron carbides give similar diffraction patterns (*9*), prevents determination of the actual carbide phase present. Regretably, AES does not provide any additional information on the identity of the carbide, as reference spectra for iron carbides do not appear to be available. High-magnification micrographs (Fig. 4c) of the coated carbide particles generally show that the graphitic carbon is poorly crystalline, although a few regions approximately 4 nm in size do show ordered stacking of the graphite layers parallel to the carbide particle surface.

In order to determine if the procedure used to passivate the CO activated sample prior to transfer to the TEM apparatus resulted in any carbon removal, AES measurements of the surface composition of a CO activated catalyst were made before and after exposure to one Torr of oxygen at 300 K. These measurements show no discernable change in the C(272 eV)/Fe(703 eV) ratio, demonstrating that little or no carbon is removed during the passivation treatment. Passivation does result in a doubling of both the K(252 eV) and O(511 eV) peak heights, suggesting that KOH, which is believed to be the potassium compound present during F–T synthesis (*27, 28*), migrates to the surface of the carbon film upon exposure to oxygen. The driving force for this migration is unknown. The behavior of potassium is discussed further below.

Using tabulated Auger sensitivity factors for carbon and iron (*26*) and assuming a uniform thickness in the C_g layer, it can be estimated (*29*) that for the sample used to

obtain the spectra in Fig. 3, the carbon overlayer thickness increases from 1 to 2 nm as activation time increases from 4 to 22 h. These estimates represent average thicknesses, and do not account for the spatial variations in the C_g layer thickness which are apparent in Fig. 4. In addition, the AES estimates are probably inflated by the presence of the graphitic carbon filaments, which contribute to the AES spectra, but not to the thickness of the carbon layer measured by TEM. The AES estimate of the C_g layer thickness following CO activation at 280°C for 22 h falls within the low end of the range of thicknesses observed in Fig. 4. Part of the difference between the AES and TEM measurements may be due to the exotherm which occurred during the initial stages of preparation of the CO activated sample for TEM (see Section 2). Supporting this explanation are AES experiments on a second sample of the 100 Fe/3 Cu/0.2 K catalyst, in which the CO activation temperature was inadvertently allowed to briefly rise above 325°C. This sample displayed C(272 eV)/Fe(703 eV) Auger ratios substantially higher than those shown in Fig. 3, suggesting that increased temperature results in greater graphitic carbon buildup and that the differences in C_g layer thickness observed between the AES and TEM experiments are due to the exotherm which occurred during TEM sample preparation. Given this possibility, as well as the uncertainties in Auger sensitivity factors and IMFP's, the agreement between C_g layer thicknesses measured by TEM and AES is satisfactory.

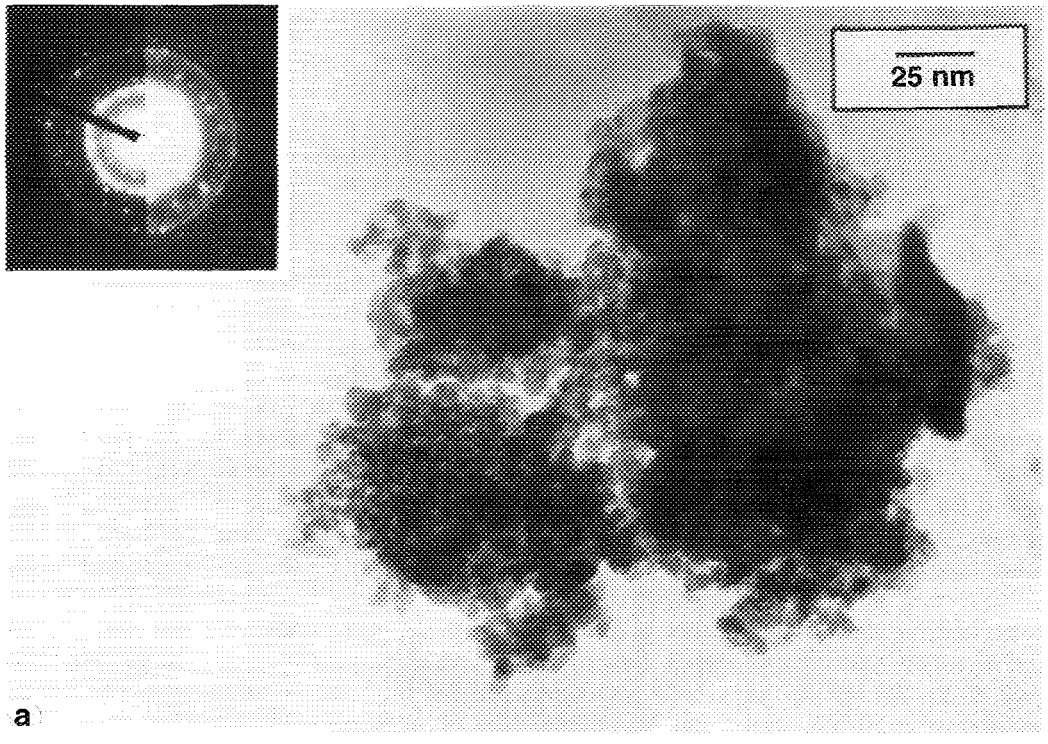

FIG. 4. (a) Transmission electron micrograph and electron diffraction pattern of the calcined 100 Fe/3 Cu/0.2 K catalyst. (b) Transmission electron micrograph and electron diffraction pattern of 100 Fe/3 Cu/0.2 K catalyst following activation in 1 atm of CO at 280°C for 24 h. (c) High-magnification transmission electron micrograph of 100 Fe/3 Cu/0.2 K catalyst following activation in 1 atm of CO at 280°C for 24 h.

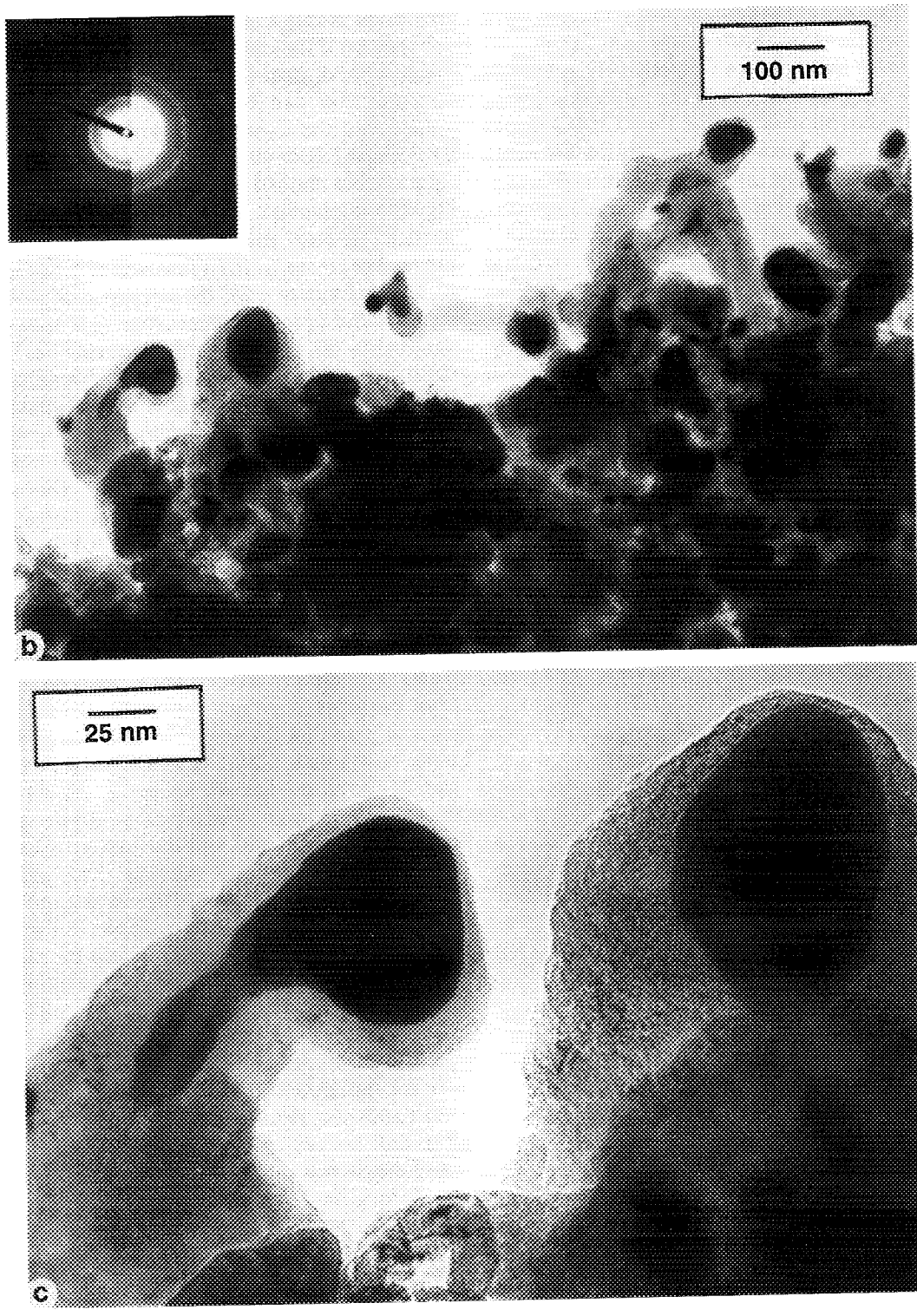

FIG. 4—*Continued*

The growth of filamentous carbon from catalytic disproportionation of CO is well known and has been extensively reviewed (*30–33*), and the filaments produced during CO activation of the 100 Fe/3 Cu/0.2 K catalyst show strong similarities to filaments reported in the literature. Although many details of the mechanism of filament growth are not yet understood, general agreement exists that filaments are formed by dissociation of CO on the surface of the catalyst, followed by diffusion of carbon through the catalyst particles and deposition at the interface between the catalyst particle and the filament (*30–36*). This mechanism requires that the leading edge of the catalyst particle be clean. Particles which have become encapsulated by a carbon overlayer are associated with filaments which have ceased to grow. As shown in Fig. 4, virtually all of the iron carbide particles seen here are encapsulated by a 2–10 nm layer of graphitic carbon, suggesting that all filament growth has stopped. In contrast to this observation are numerous TEM reports which show the presence of unencapsulated iron carbide particles located on the ends of graphitic carbon filaments grown by CO or hydrocarbon disproportionation (*30–33*). In none of these studies is potassium present on the surface, however. Since it is well established that potassium increases the rate of CO dissociation, and therefore carbon deposition, during F–T synthesis on iron catalysts (*5, 23, 25, 27, 37–39*), it is not surprising that more extensive encapsulation occurs with the 100 Fe/3 Cu/0.2 K catalyst than with pure iron catalysts.

The complete encapsulation of the catalyst particles by C_g during CO activation of the 100 Fe/3 Cu/0.2 K catalyst is not consistent with either the AES results, which show continued growth of the C(272 eV)/Fe(703 eV) AES ratio with time even after 22 h of activation, nor the activity measurements of Bukur *et al.* (*14*), which show that activation of the 100 Fe/3 Cu/0.2 K catalyst in CO at 280°C for 24 h produces a more active catalyst than any other activation treatment studied. Neither of these results is expected if the catalyst particles are truly encapsulated during CO activation. The contradiction can be resolved if it is assumed that the C_g layer formed on the 100 Fe/3 Cu/0.2 K catalyst particles is not continuous, but instead is highly porous, allowing CO molecules to reach the catalyst particle surface and dissociate or disproportionate, even in the presence of a thick C_g layer. Evidence for the presence of porosity in the C_g layer comes from BET measurements on the CO activated 100 Fe/3 Cu/0.2 K catalyst, which give a surface area of 118 m^2/g. This value is much higher than the value of ~16 m^2/g predicted from the average catalyst particle size of 50 nm and iron carbide density of 7.6 g/cm^3. There is room for error in this estimate, however, since the particle size distribution is broad, and an insufficient number of particles are visible to allow the particle size distribution to be determined with confidence. Also, only particles near the edge of the agglomerates are clearly discernable, and these edge particles may not reflect the overall particle size distribution. Finally, it is not clear how much of the additional surface area is due to the carbon filaments. Nevertheless, the large discrepancy between measured surface area and the surface area predicted from catalyst particle size certainly leaves room for porosity in the carbon layer. The electron micrographs in Fig. 4 show no evidence for pores within the C_g layer, but this could be the result of poor contrast between the pores and the solid carbon phase. Although there does not seem to be a clear precedent in the literature for the growth of a porous C_g layer on iron catalysts, results from Wesner *et al.* (*25*), and Dwyer and Hardenbergh (*6*) are intriguing in this regard. Both groups report the formation of *multilayers* of graphitic carbon during F–T synthesis on iron catalysts, and yet in both cases the catalysts still display significant F–T activity, albeit at a much lower rate than for the initially clean catalysts. Although not specifically

discussed in either of these papers, the results suggest that the C_g multilayers are porous, as proposed here. Porosity in the C_g layer could result from the relatively low temperature used in the CO activation. In most studies of carbon filament growth, temperatures of 500°C or greater are employed, which allows a more ordered stacking arrangement to be achieved by the C_g layer than can be attained at the relatively low temperature of 280°C used to activate the 100 Fe/3 Cu/0.2 K catalyst. For this reason, a layer formed at 280°C might be expected to be more porous than one formed at 500°C or higher. Indeed, high temperatures are used in the production of carbon fibers to increase the ordering and orientation of graphite crystallites, and this process is accompanied by large decreases in fiber surface area (*40*).

Figure 3 shows a pronounced increase in the Cu(920 eV)/Fe(703 eV) peak ratio with activation time. This ratio is 0.02–0.03 prior to activation, but rises to 0.20 after 22 h of activation in CO. The difference between the IMFPs of the copper and iron Auger electrons, which results in different attenuation as they pass through the carbon layer, is too small to account for the observed increase in the Cu(920 eV)/Fe(703 eV) ratio. It must therefore be concluded that segregation of copper to the catalyst surface occurs during CO activation of the 100 Fe/3 Cu/0.2 K catalyst. This segregation could be the result of the low solubility of copper in the iron carbide phase formed during CO activation. Little or no enhancement of the Cu(920 eV) peak is observed after hydrogen activation (*1*), indicating that copper segregation is not related to reduction of iron to the metallic state. In contrast to the present work, Wielers *et al.* (*41*) report that *iron* segregates to the surface of reduced (uncarbided) Fe–Cu particles upon room temperature exposure to CO. They attribute the segregation to the higher heat of adsorption of CO on iron than on copper, which provides a driving force for segregation. Given that no iron carbide was present in the Fe–Cu particles studied by Weilers *et al.* that the copper contents used in that study were substantially higher than that of the 100 Fe/3 Cu/0.2 K catalyst, and that a higher CO exposure temperature was employed here, it is perhaps not surprising that differences in segregation behavior are observed. In the absence of adsorbate effects, surface segregation results from differences in the surface tension of the two phases (*42*). With adsorbates present, differences in adsorbate binding energies also come into play. The differences between the results of Weilers *et al.* and the present work may therefore be ascribed to a difference in the heat of adsorption of CO on iron *vs* iron carbide, as well as changes in the relative surface tensions of the iron and copper phases upon carbide formation. In addition to growth of the Cu(920 eV) signal, the O(511 eV) signal in Fig. 3 also increases with CO activation time, but this effect was not reproducible.

Peaks due to sulfur and chlorine at 152 and 181 eV, respectively, are barely visible in Fig. 3, as are small peaks at 383 and 420 eV which are due to titania contamination from the die used to press the samples. The titania contamination does not affect the results, as discussed in the previous paper (*1*). Chlorine contamination was not observed following hydrogen activation of the 100 Fe/3 Cu/0.2 K catalyst, and must therefore be related to the presence of CO in the reactor. The most likely possibility is that CO induces outgassing of chlorine from a viton O-ring used in the gate valve which isolates the reactor from the surface analysis chamber. If so, then the presence of chlorine can safely be ignored as the result of an experimental artifact. The presence of sulfur, however, cannot be ignored. Sulfur arises from bulk sulfate impurities present in the 100 Fe/3 Cu/0.2 K catalyst, which segregate to the catalyst surface during activation. This process has been discussed in detail in the preceding paper on hydrogen activation of F–T catalysts (*1*). If the sulfur resides on the surface of the iron carbide

particles, beneath the C_g layer, then the large difference in IMFP between the S(152 eV) and Fe(703 eV) Auger electrons in carbon (*15*) (0.5 nm *vs* 1.06 nm) would mean that the S(152 eV)/Fe(703 eV) ratio would be attenuated by the presence of the C_g overlayer. Unfortunately, the nonuniform thickness of The C_g overlayer (see Fig. 4) prevents an accurate correction for this attenuation. A rough estimate can be made, however, based on the average thickness of ~2 nm measured by AES for the 100 Fe/3 Cu/0.2 K catalyst activated in CO for 22 h (see above). A C_g overlayer of 2 nm would attentuate the S(152 eV)/Fe(703 eV) ratio by a factor of 8. Using this attenuation to adjust the measured S(152 eV)/Fe(703 eV) ratio of 0.06 gives a corrected value of 0.48. The use of tabulated Auger sensitivity factors (*26*) and the quantification method of Briggs and Seah (*29*) shows that a S(152 eV)/Fe(703 eV) ratio of 0.48 corresponds to a sulfur surface coverage of 0.2 monolayers (ML). In the previous paper (*1*) it was argued that sulfur coverages of this magnitude can have an adverse effect on F–T activity. It therefore appears that sulfur poisoning may be an important factor in determining the activity of the CO activated 100 Fe/3 Cu/0.2 K catalyst.

The K(252 eV)/Fe(703 eV) ratio does not change appreciably as the C_g layer grows. Clearly, given the short IMPF of 252-eV electrons in carbon (0.65 nm) relative to 703-eV electrons (1.06 nm) (*15*), significant attenuation of the K(252 eV)/Fe(703 eV) ratio would be expected as the thickness of the C_g layer increases, if the potassium resides at the interface between the iron carbide and the C_g layer. Since this attenuation is not observed, it must be concluded that at least a portion of the potassium is either incorporated into the carbon layer, or is adsorbed on top of the carbon. The possibility of potassium being located on top of a carbon overlayer was first raised by Bonzel and Krebs (*37*), who noted that the K 2p XPS signal did not decrease as the C 1s signal grew in during F–T synthesis on an iron foil.

3.2.2. Comparison with the literature. Comparison of the AES results obtained here with the XPS results of Li (*3*) shows good agreement. Li states that quantitative reduction of the iron to the metallic state occurs upon activation of a 100 Fe/3 Cu/0.2 K catalyst in CO at 300°C for 12 h. No mention is made, however, of the possibility of carbide formation. Since iron carbide and metallic iron have very similar Fe 2*p* XPS spectra (*6, 17*), it seems likely that the phase which Li identifies as metallic iron is in fact iron carbide. The Fe $2p_{3/2}$ peak of iron carbide is only 0.3 eV higher than that of metallic iron, and the peak shapes of iron and iron carbide are nearly identical. The C 1*s* region measured by Li shows a single peak at ~283 eV, with an unresolved shoulder on the high-energy side. The binding energy of 283 eV is characteristic of iron carbides (*6, 43*), lending further support to the argument that Li observed iron carbide rather than metallic iron. The shoulder on the high energy side of the C 1s peak can be attributed to graphitic carbon. The fact that Li was able to observe carbidic carbon, while no carbidic carbon was observed in the present work may be due to the greater escape depth of C 1*s* electrons compared to carbon Auger electrons. With the Al $K\alpha$ X-ray source used by Li, the C 1*s* electrons would have a kinetic energy of 1023 eV and an IMFP of 1.4 nm, *vs* an IMFP of only 0.65 nm for the C(272 eV) Auger electrons (*15*). It is also possible that the graphitic carbon layer in Li's work was thinner than in the present work due to differences in activation temperature and time.

The observation of a graphitic carbon layer residing on top of an iron carbide phase is not unique to the 100 Fe/3 Cu/0.2 K catalyst. Copperthwaite *et al.* (*44*), exposed a reduced iron oxide catalyst, promoted with K, CaO, MgO, Al_2O_3, and SiO_2, to CO at 250°C, and observed the formation of a graphitic carbon peak by XPS. No carbidic carbon was detected, yet the Fe $2p_{3/2}$ peak energy shifted upwards by 0.4 eV, indicating carbide formation. Apparently, the C_g layer was thick enough to completely

attenuate the C 1*s* photoelectrons from the carbide. Bonzel and co-workers (*7, 25, 37*), and Dwyer and co-workers (*6, 27, 45*) observe the growth of graphitic carbon layers on iron carbide during F–T synthesis over model iron catalysts. Studies of graphitic carbon filament growth on iron catalysts indicate that carbide formation is a prerequisite to filament formation (*30–36*). In fact, there do not appear to be any examples in the literature of growth of graphitic carbon layers on iron catalysts without accompanying formation of iron carbide. It therefore appears that formation of graphitic carbon on iron carbide is a general phenomenon for iron F–T catalysts, occurring either during CO activation or under actual F–T synthesis conditions.

3.2.3. Comparison of CO and hydrogen activation. Activation in CO at 280°C results in better F–T synthesis performance for the 100 Fe/3 Cu/0.2 K catalyst than any other activation treatment tested by Bukur *et al.* (*14*) (see Table 1). In fixed bed reactor tests initial CO conversions of 80% are achieved for both 8- and 24-h activation times. The best hydrogen activation procedure, 250°C for 8 h, gives an initial CO conversion of only 65%. Selectivity of the CO activated catalyst is also superior to that of the hydrogen activated catalysts, with the CO activated catalysts forming fewer C_1–C_5 hydrocarbons and more C_{12}^+ hydrocarbons than any hydrogen activated catalyst.

Given that CO activation of the 100 Fe/3 Cu/0.2 K catalyst results in surface properties which are vastly different from those resulting from hydrogen activation, it is not surprising that differences in F–T performance are observed. While hydrogen activation results in a metallic iron surface covered by varying amounts of sulfur, depending on activation temperature and time (*1*), CO activation results in iron carbide particles covered by a thick, porous, graphitic carbon layer, which prevents an accurate determination of surface composition. Since CO disproportionation is responsible for the growth of the C_g layer, it is probable that the CO activation results in a mixed oxide/carbide phase on the surface rather than a pure carbide, but no direct evidence exists for this conclusion. The potassium and sulfur coverages at the surface following CO activation are also problematic, as discussed earlier. The surface composition differences between CO and hydrogen activation may not be as significant as they first appear since a conditioning period was used between activation and activity measurements (*14*). This conditioning period consisted of gradually raising the reactor temperature from 190 to 250°C over a period of 30 h while flowing a H_2/CO mixture over the catalyst at the same flow rate and pressure as used in the activity measurements. Under these conditions it is quite likely that the metallic iron particles produced by hydrogen activation become carbided, and that a mixed oxide/carbide phase is formed on the surface along with some hydrocarbon fragments. Still, hydrogen activation never involves exposure to pure CO, and the temperatures reached during the conditioning period are not as high as those used during CO activation. Thus, it is likely that some surface composition differences exist even after the conditioning period.

In addition to differences in BET surface area result from the different activation procedures. Hydrogen activation results in surface areas of 10 m^2/g or less, while a relatively high surface area of 118 m^2/g is retained following CO activation. The surface area following CO activation is divided between the carbon filaments, the porous carbon layer, and exposed surfaces of the iron carbide particles. Unfortunately, the relative contributions of the different phases to the total surface area is unknown.

The numerous differences in surface composition and catalyst morphology make it difficult to pinpoint a single cause for the higher activity and better selectivity of the CO activated catalyst relative to the hydrogen activated catalyst. Because of the uncertainties regarding surface composition following CO activation, the best that can

be said at this point is that the relative F–T activity of the CO and hydrogen activated catalysts is determined by the interplay between the total surface area available for reaction, and the surface composition, which determines the activity per unit area of available surface.

3.3. Comparison of 100 Fe/5 Cu/4.2 K/25 SiO_2 and 100 Fe/3 Cu/0.2 K Catalysts

As pointed out in the Introduction, the 100 Fe/5 Cu/4.2 K/25 SiO_2 catalyst is quite insensitive to activation conditions, while the 100 Fe/3 Cu/0.2 K catalyst displays wide variations in activity as activation conditions are changed. This difference in sensitivity to activation conditions is related to the reduction behavior of the two catalysts, as discussed in the previous paper for hydrogen activation (*1*). Similar arguments apply to CO activation. The high potassium and silica content of the 100 Fe/5 Cu/4.2 K/25 SiO_2 catalysts prevents reduction of iron to the metallic state during CO activation, such that only partial reduction to Fe_3O_4 or Fe_xO is observed. As a result, CO dissociation is unfavorable and no measurable carbon buildup occurs on the surface of the 100 Fe/5 Cu/4.2 K/25 SiO_2 catalyst. Thus, the surface composition, and therefore the F–T activity, of the CO activated catalyst is quite similar to that of the hydrogen activated catalysts. In contrast, the iron in the 100 Fe/3 Cu/0.2 K catalyst is easily reduced to the metallic state, and CO dissociation is quite facile. Carbide formation and growth of a carbonaceous overlayer can therefore occur, resulting in a surface composition distinct from that formed during hydrogen activation. As a result, F–T activity and selectivity following CO activation are very different from the activity and selectivity resulting from hydrogen activation.

4. CONCLUSIONS

The surface compositions of two different iron F–T catalysts have been measured following activation in CO at 280°C. For a 100 Fe/5 Cu/4.2 K/25 SiO_2 catalyst, the surface composition after CO activation is nearly identical to the surface composition following activation in hydrogen at either 220 or 280°C (*1*). This result is consistent with F–T activity measurements which show that activity is independent of activation treatment (*13*). Only partial reduction of iron to Fe_3O_4 or Fe_xO is observed for this catalyst, and as a result, no measurable carbon deposition occurs. For a 100 Fe/3 Cu/0.2 K catalyst, the surface composition following CO activation is quite different from that following hydrogen activation. While hydrogen activation results in a surface consisting of metallic iron with varying amounts of sulfur depending on activation temperature and time, CO activation results in formation of iron carbide particles covered by a thick, porous, graphitic carbon overlayer which prevents an accurate determination of the surface composition. The differences between CO and hydrogen activation are consistent with activity measurements (*14*) which show that the CO activated catalyst is more active for F–T synthesis than any of the hydrogen-activated catalysts. The relative activities of the hydrogen- and CO-activated catalysts are determined by the interplay between accessible surface area and intrinsic surface activity, which varies with surface composition.

ACKNOWLEDGMENTS

We thank Professor Dragomir Bukur of Texas A&M University for providing the catalyst samples used in this work, as well as for many stimulating discussions. The technical assistance of Elaine Boespflug is also gratefully acknowledged. Support for this work was provided by the Fossil Energy Division of the U.S. Department of Energy.

REFERENCES

1. Sault, A. G., *J. Catal.* **140,** 121–135 (1993).
2. Storch, H. H., Golumbic, N., and Anderson, R. B., "The Fischer–Tropsch and Related Synthesis," p. 28. Wiley, New York, 1951.
3. Li, C., "Effect of Potassium and Copper Promoters on Reduction Behavior of Precipitated Iron Catalysts." Ph.D. thesis, Texas A&M University, 1988.

4. Leith, L. R., and Howden, M. G., *Appl. Catal.* **37,** 75 (1988).
5. Richard, M. A., Soled, S. L., Fiato, R. A., and DeRites, B. A., *Mater. Res. Bull.* **18,** 829 (1983).
6. Dwyer, D. J., and Hardenbergh, J. H., *J. Catal.* **87,** 66 (1984).
7. Krebs, H. J., and Bonzel, H. P., *Surf. Sci.* **99,** 570 (1980).
8. Niemantsverdriet, J. W., and van der Kraan, A. M., *J. Catal.* **72,** 385 (1980).
9. Niemantsverdriet, J. W., van der Kraan, A. M., van Dijk, W. L., and van der Baan, H. S., *J. Phys. Chem.* **84,** 3363 (1980).
10. Amelse, J. A., Butt, J. B., and Schwartz, L. H., *J. Phys. Chem.* **82,** 558 (1978).
11. Raupp, G. B., and Delgass, W. N., *J. Catal.* **58,** 361 (1979).
12. Kuivila, C. S., Stair, P. C., and Butt, J. B., *J. Catal.* **118,** 299 (1989).
13. Bukur, D. B., Ledakowicz, S., and Rama Krishna, M., *in* "Indirect Liquefaction Contractors' Review Meeting Proceedings" (G. J. Steigel and R. D. Srivastava, Eds.), p. 221. U.S. Department of Energy, Pittsburgh Energy Technology Center, Pittsburgh, 1990. (Available form the National Technical Information Service, U.S. Dept. of Commerce, Springfield, VA 22161.)
14. Bukur, D. B., Lang, X., Rossin, J. A., Zimmerman, W. H., Rosnyek, M. P., Yeh, E. B., and Li, C., *Ind. Eng. Chem. Res.* **28,** 1130 (1989).
15. Seah, M. P., and Dench, W. A., *Surf. Interface Anal.* **1,** 2 (1979).
16. Lox, E. S., Marin, G. B., DeGrave, E., and Bussiere, P., *Appl. Catal.* **40,** 197 (1988).
17. Kuivila, C. S., Butt, J. B., and Stair, P. C., *Appl. Surf. Sci.* **32,** 99 (1988).
18. Arbab, M., and Hudson, J. B., *Surf. Sci.* **206,** 317 (1988).
19. Simmons, G. W., and Dwyer, D. J., *Surf. Sci.* **48,** 373 (1975).
20. Miyano, T., Sakisaka, Y., Komeda, T., and Onchi, M., *Surf. Sci.* **169,** 197 (1986).
21. Seo, M., Lumsden, J. B., and Staehle, R. W., *Surf. Sci.* **50,** 541 (1975).
22. Rankin, J. L., and Bartholomew, C. H., *J. Catal.* **100,** 533 (1986).
23. Dry, M. E., *in* "Applied Industrial Catalysis," Vol. 2, p. 167. Academic Press, New York, 1983.
24. Dalmon, J.-A., Dutartre, R., and Martin, G.-A., *C. R. Acad. Sci. Ser. C.* **287,** 557 (1978).
25. Wesner, D. A., Coenen, F. P., and Bonzel, H. P., *Langmuir* **1,** 478 (1985).
26. Davis, L. E., McDonald, N. C., Palmberg, P. W., Riach, G. E., and Weber, R. E., "Handbook of Auger Electron Spectroscopy." Perkin–Elmer Corp., Eden Prairie, MN, 1978.
27. Dwyer, D. J., and Hardenbergh, J. H., *Appl. Surf. Sci.* **19,** 14 (1984).
28. Bonzel, H. P., Broden, G., and Krebs, H. J., *Appl. Surf. Sci.* **16,** 373 (1983).
29. Briggs, D., and Seah, M. P., "Practical Surface Analysis by Auger and X-ray Photoelectron Spectroscopy," Chap. 5. Wiley, New York, 1983.
30. Dresselhaus, M. S., Dresselhaus, G., Sugihara, K., Spain, I. L, and Goldberg, H. A., "Graphite Fibers and Composites," Chap. 2 and 3. Springer-Verlag, New York, 1988.
31. Baker, R. T. K., *in* "Chemistry and Physics of Carbon" (P. L. Walker, Jr., and P. A. Thrower, Eds.), Vol. 14, p. 83. Dekker, New York, 1978.
32. Baker, R. T. K., *in* "Carbon Fibers, Filaments, and Composites (J. L. Figueiredo, C. A. Bernardo, R. T. K. Baker and K. J. Huttinger, Eds.), p. 405. Kluwer, Boston, 1990.
33. Sacco, A., Jr., *in* "Carbon Fibers, Filaments, and Composites" (J. L. Figueiredo, C. A. Bernardo, R. T. K. Baker and K. J. Huttinger, Eds.), p. 459. Kluwer, Boston, 1990.
34. Alstrup, I., *J. Catal.* **109,** 241 (1988).
35. Sacco, A., Jr., Thacker, P., Chang, T. N., and Chiang, A. T. S., *J. Catal.* **85,** 224 (1984).
36. Rostrup-Nielsen, J., and Trimm, D. L., *J. Catal.* **48,** 155 (1977).
37. Bonzel, H. P., and Krebs, H. J., *Surf. Sci.* **109,** L527 (1981).
38. Rao, V. U. S., Steigel, G. J., Cinquegrane, G. J., and Srivastava, R. D., *Fuel Process. Technol.* **30,** 83 (1992).
39. Frohning, C. D., *in* "New Syntheses with Carbon Monoxide" (J. Falbe, Ed.), p. 353. Springer-Verlag, New York, 1980.
40. Donnet, J-B., and Bansal, R. C., "Carbon Fibers," p. 112–113. Dekker, New York, 1984.
41. Weilers, A. F. H., Hop, C. E. C. A., van Beijnum, J., van der Kraan, A. M., and Geus, J. W., *J. Catal.* **121,** 364 (1990).
42. Zangwill, A., "Physics at Surfaces," p. 87. Cambridge Univ. Press, New York, 1988.
43. Bonzel, H. P., and Krebs, H. J., *Surf. Sci.* **91,** 499 (1980).
44. Copperthwaite, R. G., Loggenberg, P. M., Derry, T. E., and Sellschop, J. P. F., *Vacuum* **38,** 413 (1988).
45. Wachs, I. E., Dwyer, D. J., and Iglesia, E., *Appl. Catal.* **12,** 201 (1984).